Fluorine-18-Fluorodeoxyglucose Cardiac Imaging Using a Modified Scintillation Camera

Martin P. Sandler, Jeroen J. Bax, James A. Patton, Frans C. Visser, William H. Martin and William Wijns

Department of Radiology and Radiological Sciences, Vanderbilt University Medical Center, Nashville, Tennessee; Department of Cardiology, University Hospital, Leiden, The Netherlands; Department of Cardiology, Free University Hospital, Amsterdam, The Netherlands; and Cardiovascular Center, Aalst, Belgium

Conventional ^{201}Tl and hexakis 2-methoxy-2-isobutyl isonitrile studies are less accurate as compared to FDG PET in the prediction of functional recovery after revascularization in patients with injured but viable myocardium. The introduction of a dual-head variable-angle-geometry scintillation camera equipped with thicker crystals ($\frac{5}{8}$ in.) and high-resolution, ultrahigh-energy collimators capable of 511 keV imaging has permitted FDG SPECT to provide information equivalent to that of PET for the detection of injured but viable myocardium in patients with chronic ischemic heart disease. The development of standardized glucose-loading protocols, including glucose-insulin-potassium infusion and the potential use of nicotinic acid derivatives, has simplified the method of obtaining consistently good-to-excellent quality FDG SPECT cardiac studies. FDG SPECT may become the modality of choice for evaluating injured but viable myocardium because of enhanced availability of FDG, logistics, patient convenience, accuracy and cost-effectiveness compared to PET.

Key Words: fluorodeoxyglucose; cardiac; SPECT

J Nucl Med 1998; 39:2035–2043

The identification of hibernating myocardium in patients with poor ventricular function has become increasingly important as investigators demonstrate an improvement in ventricular performance in patients with injured but viable myocardium who undergo revascularization (*1–8*). Modifications of ^{201}Tl redistribution protocols and rest/stress ^{99m}Tc-labeled hexakis 2-methoxy-2-isobutyl isonitrile (MIBI) perfusion studies continue to underestimate viability compared to perfusion/metabolic imaging with ^{13}N-ammonia or ^{82}Rb/^{18}F-labeled fluorodeoxyglucose (FDG) PET (*9*).

Advances in scintigraphic camera technology (*10–18*) combined with data from numerous investigators have demonstrated that FDG SPECT used in combination with cardiac perfusion agents, either sequentially (*17,19*) or with dual-isotope simultaneous acquisition (DISA) (*20,21*), provides an acceptable alternative to PET for the detection of injured but viable myocardium.

The purpose of this article is to describe the state-of-the-art imaging characteristics and capabilities of modified scintillation cameras to perform cardiac FDG SPECT. Topics discussed include camera modifications, ultrahigh-energy collimation, single-head versus 90° dual-head collimation, coincidence counting techniques, patient preparation, imaging protocols and outcome data.

Received Feb. 3, 1998; revision accepted May 26, 1998.

For correspondence or reprints contact: Martin P. Sandler, MD, Department of Radiology and Radiological Sciences, Vanderbilt University Medical Center, 21st Ave. South and Garland, Nashville, TN 37232-2675.

CAMERA MODIFICATIONS

In recent years, manufacturers have devoted much effort to the optimization of the scintillation camera for low-energy imaging, since a vast majority of nuclear medicine procedures involve radionuclides with energies below 200 keV. The need for imaging of 511 keV photons has made it necessary to reverse some of these efforts and/or apply the technology that was developed for low-energy imaging to high-energy imaging applications.

The first step in this process was to expand the pulse-height-analyzer energy range of the scintillation camera. Some manufacturers have introduced a high-energy mode by simply reducing the high voltage and recalibrating the pulse-height analyzer. Due to the difficulty in resolving the low-energy peak from the noise (caused by the reduction in gain), this resulted in some difficulty in imaging at low energies (e.g., 70 keV for ^{201}Tl) when simultaneous imaging of low and high energies was desired. Some systems can acceptably resolve the 70 keV peak of ^{201}Tl, but there is still the problem of interference of lead x-rays and the effect of reduced activity of ^{201}Tl (4–5 mCi) as compared to ^{99m}Tc (10–25 mCi) used in myocardial imaging. However, acceptable simultaneous imaging at 140 and 511 keV has been accomplished using this technique (*22*).

The energy dependence of flood-field uniformity is well known, and manufacturers have typically used low- and medium-energy linearity and sensitivity correction maps to provide images of excellent uniformity throughout the diagnostic range. Extending the diagnostic range to 511 keV therefore requires linearity and sensitivity correction maps in the high-energy range. This can be done by simply using the medium-energy maps but is better accomplished by generating new high-energy maps. Some manufacturers use a combination of the two (e.g., medium-energy linearity maps and high-energy sensitivity maps).

COLLIMATED SINGLES COUNTING WITH SPECT

Collimator design for high-energy imaging with SPECT is relatively straightforward. First, it is necessary to significantly increase septal thickness to absorb the high-energy photons. For adequate sensitivity, the hole diameters must be increased, and to maintain reasonable spatial resolution, the hole length must be increased (*22*). These modifications typically result in very heavy collimators with low sensitivity and medium resolution as compared to conventional low-energy, high-resolution collimators. Table 1 shows a summary of the range of parameters reported for currently available collimators. In reviewing these parameters, it must be observed that the quoted septal penetration values are calculated for a single septum. Septal penetration may actually account for 30%–50% of detected events in a clinical situation.

Initially, there was some concern about the capability and mechanical stability of the camera gantries when using high-

TABLE 1
Parameters of Currently Available Collimators

Collimator	Weight (lb)	FWHM at 10 cm (mm)	Sensitivity (cpm/μCi)	Septal penetration (%)	Septal thickness (mm)	Hole length (mm)	Hole diameter (mm)
LE	88	7.2	160	0.2	0.2	35	1.5
HE	224–475	8.2–17.0	43–150	3.9–7.3	1.7–3.4	60–104	2.5–5.1

LE = Elscint low-energy, high-resolution collimator; HE = high-energy collimator; FWHM = full width at half maximum.

energy collimators weighing in excess of 300 lb (136.4 kg) each and the additional shielding that may be necessary for high-energy imaging. Current systems appear to support this additional weight adequately without modifications to the gantries. However, it is important to measure the center of rotation (COR) using the high-energy collimators and routinely to perform COR corrections, if necessary.

Radiation leakage through the detector housing is also of concern when imaging high-energy photons, especially in older systems being upgraded to perform 511 keV imaging, and leakage testing should be performed before accepting a system for high-energy imaging applications. Manufacturers are now fabricating systems with shielding designed for high-energy imaging.

CRYSTAL THICKNESS

Currently available scintillation cameras typically use $\frac{3}{8}$ in. (9.525 mm) thick NaI(Tl) crystals because of their excellent intrinsic spatial resolution. The system in use at Vanderbilt University Medical Center (VariCam; Elscint Ltd., Haifa, Israel) has a 3.8 mm full width at half maximum (FWHM) at 140 keV. However, although crystals of this thickness have a photopeak efficiency of approximately 84% at 140 keV, the photopeak efficiency at 511 keV is approximately 13%. Recently, because of the demand for increased efficiencies at 511 keV, manufacturers have increased the crystal options to $\frac{1}{2}$ (12.7 mm), $\frac{5}{8}$ (15.875 mm) and $\frac{3}{4}$ in. (19.05 mm). Table 2 shows the approximate increase in the photopeak efficiencies of a $\frac{5}{8}$ in. crystal at the energies commonly used for imaging, compared to those of the $\frac{3}{8}$ in. crystal (e.g., the measured increase in photopeak efficiency of a $\frac{5}{8}$ in. crystal is 10% higher than that for a $\frac{3}{8}$ in. crystal). The relative intensities of the multiple energies of ^{67}Ga and ^{111}In are taken into consideration in these calculations.

If high-energy imaging were the only goal, obviously the thicker the crystal the better. However, increasing crystal thickness typically results in degraded intrinsic spatial resolution at lower energies. Recent data indicate that these degradations are not clinically significant (Table 3) because although the intrinsic spatial resolution of ^{201}Tl and ^{99m}Tc is degraded by 0.5 mm, the extrinsic spatial resolution with a low-energy, high-resolution collimator is only degraded by 0.2 mm at 10 cm from the collimator face.

DUAL-HEAD CAMERAS

Imaging studies with phantoms and in patients comparing 180° versus 360° SPECT image acquisition of the myocardium have shown that superior image resolution is obtained with 180° acquisition (*16*), as is the case for ^{201}Tl and ^{99m}Tc imaging protocols. Thus, dual-head cameras with fixed 180° geometries have limited advantages over single-head cameras for this application. However, dual-head cameras in a 90° geometry (either fixed or variable) provide twice the sensitivity of a single-head camera for 180° acquisition. This added sensitivity permits the use of new high-energy collimators with improved spatial resolution (and reduced sensitivity). High-energy collimators are now in use that have the same spatial resolution at 140 keV as the low-energy, high-resolution collimators commonly used for the imaging of low-energy photon emitters. This added sensitivity also permits the performance of simultaneous, dual-isotope gated SPECT, which makes it possible to evaluate ischemia, metabolism, wall motion and ejection fraction from a single data acquisition.

COINCIDENCE IMAGING

The recent introduction of coincidence imaging capabilities using a dual-head scintillation camera has created much interest. Coincidence imaging is accomplished with the detectors positioned at 180° with electronic collimation (coincidence timing window) used to simultaneously detect an annihilation photon resulting from a positron decay (the technique used in PET) in each detector. This process places significant demands on camera electronics because many singles events are being recorded in each camera as both primary and scattered photons interact with the detector. Typically fewer than 1% of the detected events are the result of true coincidences. Therefore, at least 1 million cps must be recorded in each detector to be able to detect 10,000 coincidences per second. Also as the counting rate rises, the possibility of random coincidences increases. Thus, the camera must be capable of handling extremely high counting rates, and the timing window must be very small (typically 15 nsec).

Currently, coincidence imaging with the scintillation camera is performed using either a two-dimensional or three-dimensional approach. In two-dimensional imaging, slit (septa) collimators (slits positioned perpendicular to the imaging table) with graded absorbers are used to reduce the singles rate from activity outside of the region of interest (ROI) and to reduce the

TABLE 2
Predicted and Measured Increases in Efficiency Due to Increased Crystal Thickness ($\frac{3}{8}$–$\frac{5}{8}$ in.)

Crystal Thickness	^{201}Tl	^{99m}Tc	^{111}In	^{67}Ga	^{131}I	^{18}F
Predicted	0%	13%	29%	11%	50%	62%
Measured	0%	10%	—	—	—	100%

TABLE 3
Intrinsic Spatial Resolutions (FWHM of line source of fluorine) for $\frac{3}{8}$- and $\frac{5}{8}$-in. Thick NaI(Tl) Crystals

Isotope	Energy (keV)	Resolution for $\frac{3}{8}$-in. crystal (mm)	Resolution for $\frac{5}{8}$-in. crystal (mm)
^{201}Tl	70	5.6	6.1
^{99m}Tc	140	3.8	4.3

FWHM = full width at half maximum.

effects of low-energy scattered radiation. The graded absorbers are thin sheets of lead, copper and tin that preferentially absorb low-energy photons, preventing these photons from reaching the crystal and inflating the counting rate. Coincidence events are recorded from relatively thick (1–2 cm) transverse slices as the detector heads rotate around the patient. In the three-dimensional approach, only graded absorbers may be used to absorb low-energy photons, and acquisition is not limited along the z-axis (axis of the imaging table). Tomographic image reconstruction is accomplished by using iterative reconstruction techniques or by reformatting the data into planar projection arrays and then using routine filtered backprojection algorithms. The use of multiple-pulse-height analyzer windows during acquisition to record Compton-scattered events as well as photopeak events occurring in the detectors makes it possible to increase the sensitivity of the techniques. The three-dimensional technique has the advantage of sensitivity over two-dimensional techniques using septa collimators because of the removal of the septa collimators and an increase in the axial acceptance angle to the maximum value, permitting a three-dimensional acquisition. In the two-dimensional technique with septa, the axial acceptance angle is small (e.g., 8°), and acquisition is limited to a series of thick transaxial slices. On the other hand, two-dimensional techniques may provide images of higher contrast due to reduced singles rates from activity outside of the ROI as well as reduced random coincidence rates. The singles rate is reduced by absorption of photons in the lead septa; therefore, the randoms are reduced since they depend on the singles rate. Current capabilities provide the spatial resolution of PET with improved sensitivity over that of collimated single photon imaging but still less than that of modern PET scanners.

ARTIFACTS

As stated earlier, one of the primary applications of high-energy imaging is the simultaneous acquisition of images of two radionuclide distributions (specifically ^{99m}Tc and ^{18}F). Using general-purpose, high-energy collimators, one may obtain acceptable diagnostic images of the myocardium from both ^{99m}Tc and ^{18}F distributions, although the spatial resolution at 140 keV is worse than that of low-energy, high-resolution collimators. Because of the increased sensitivity gained by using dual-head, variable-angle-geometry scintillation cameras with $\frac{5}{8}$ in. crystals oriented at 90°, high-resolution, high-energy collimators can be used for imaging. Spatial resolutions comparable to those of low-energy, high-resolution collimators can be obtained at 140 keV and are only slightly degraded at 511 keV, since the myocardium is typically imaged using a 180° rather than a 360° acquisition, as described above.

One concern about the dual-isotope technique is the contribution to the ^{99m}Tc window from downscatter caused by the presence of ^{18}F. Phantom measurements performed on a cardiac

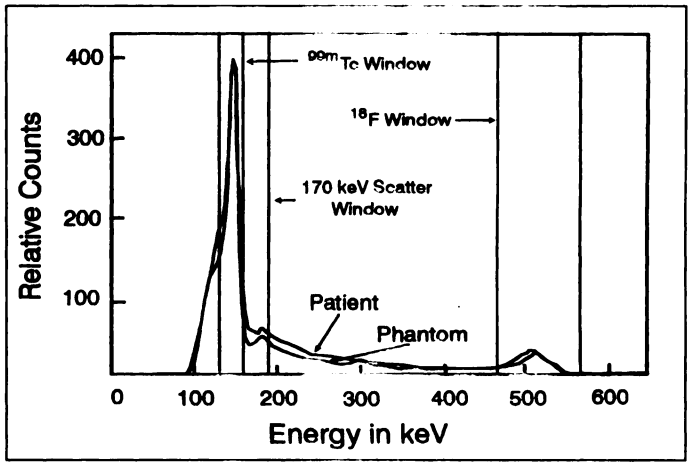

FIGURE 1. Energy spectra from cardiac phantom containing distributions of ^{99m}Tc and ^{18}F with an activity ratio of 3.2:1. The 20% windows at 140 and 511 keV were used for imaging, and 20% window at 170 keV was used for downscatter correction.

phantom containing a solution of ^{99m}Tc and ^{18}F in a 3.2:1 ratio (the minimum ratio anticipated at the time of imaging) in the myocardium from the administration of 25 mCi ^{99m}Tc-MIBI and 10 mCi FDG showed that the downscatter contributed only 5.9% of the total counts in the ^{99m}Tc window. The contribution of ^{99m}Tc photons to the downscatter window were 5% of the total counts (*20*). In five patients who underwent DISA SPECT and were judged to have normal distributions of both radiopharmaceuticals in the absence of disease (confirmed by coronary angiography), the contribution of ^{18}F was 3.7% or 6.6% of the total counts in the ^{99m}Tc window (*20*). Thus, in patients with normal global perfusion and normal metabolism, the downscatter effect was judged to be insignificant. However, in patients with ischemic heart disease manifested by decreased global perfusion and/or increased metabolism, the possibility exists for errors in the quantification of ischemic regions (*22*).

To further evaluate this effect, a downscatter correction was implemented. To correct for the downscatter of ^{18}F into the ^{99m}Tc window, a third window, first described by Yang et al. (*23*), was added to the DISA protocol using a 20% window centered on the 170 keV backscatter peak (Fig. 1). Cardiac phantom measurements using only ^{18}F were obtained to determine the fraction of the scatter window counts (scatter factor) that were recorded in the 20% ^{99m}Tc window at 140 keV. Phantom measurements using only ^{99m}Tc were also obtained to determine the contribution of ^{99m}Tc to the scatter window. The image-processing protocol was modified to provide a set of scatter-corrected SPECT MIBI images in addition to the routine FDG images and uncorrected MIBI images. The corrected images were obtained by first using the scatter window counts and the scatter factor to determine the number of counts to subtract from the ^{99m}Tc window on a projection-by-projection basis, and then images were reconstructed after the routine protocol. Twenty-five patients were studied using the DISA protocol with the scatter correction in place. Uncorrected and scatter-corrected SPECT images were presented at the daily clinical review session at Vanderbilt University Medical Center, in which nuclear medicine physicians and cardiologists reviewed the results. This study showed that there was no difference in diagnostic information content in the corrected versus uncorrected images.

Simultaneous imaging of ^{201}Tl and ^{18}F is more complex. The low-energy (70 keV) of ^{201}Tl and the lower activities commonly used (2–4 mCi) make the downscatter effect more

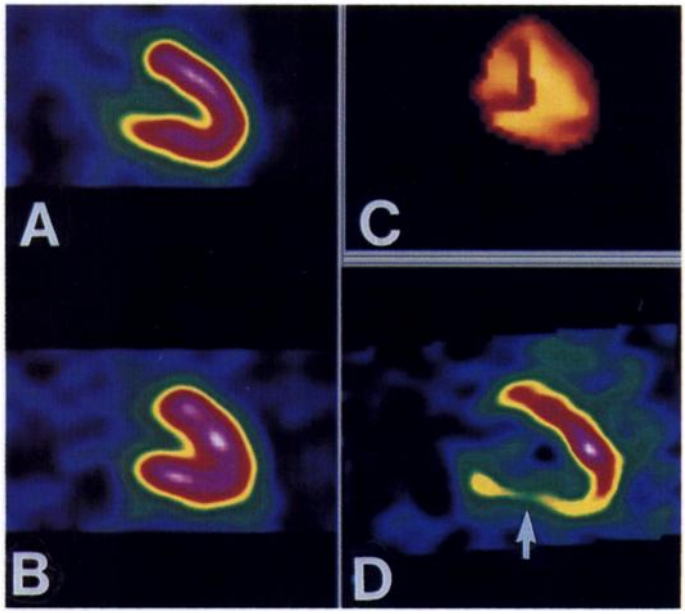

FIGURE 2. A 59-yr-old woman with history of left anterior descending coronary artery disease and stenting was referred for DISA SPECT after an episode of acute chest pain. Stress ^{99m}Tc-MIBI (A) and rest FDG ventrical long-axis (B) images obtained with fixed dual-head camera demonstrate normal study. (C) Three-dimensional ^{99m}Tc-MIBI image reconstruction confirms normal myocardial perfusion. (D) Dual-head coincidence images obtained before DISA SPECT demonstrate diminished inferior wall metabolic activity (arrow) secondary to attenuation artifact.

significant, and the energy recalibration used for high-energy imaging often makes it difficult to effectively resolve the ^{201}Tl photopeak, as previously described.

Attenuation of photons from the inferior wall of the left ventricle (LV) by the diaphragm frequently results in an artifact with cardiac SPECT. This is more apparent with low-energy photon emitters such as ^{201}Tl and ^{99m}Tc and may result in a misdiagnosis of ischemia. One approach to identifying this problem is to image the patient in the prone position, in addition to the routine supine position, and to compare the two sets of images. Attenuation of the inferior wall may occur in the prone position but will generally be reduced compared to supine imaging. A second approach is to use an external source to obtain a transmission image that can then be used to perform an attenuation correction of the emission data from ^{99m}Tc. Several manufacturers are now offering either a fixed or scanning line source (usually ^{153}Gd) to perform this correction geometrically. In dual-isotope studies, it is possible to collect simultaneously emission data from the distribution of the two radionuclides and transmission data from the external source so that additional imaging time is not required.

Attenuation of 511 keV photons in SPECT imaging is not as significant as for low-energy photon imaging. However, this is not the case in coincidence imaging (Fig. 2) because it requires the simultaneous detection of the annihilation photons that result from positron decay. Therefore, both photons must pass through the patient without interaction, and the probability of the occurrence is less than that for only one of the photons. The methods for attenuation correction of coincidence data in PET are well known (*24*), and these techniques are now being developed for use with dual-head-camera coincidence imaging. In the absence of attenuation correction, superior cardiac image quality is seen with SPECT versus dual-head coincidence (DHC).

PATIENT PREPARATION

Because glucose plays a critical role in the metabolism of the ischemic myocardium, the glucose analog FDG is frequently used for clinical imaging. FDG competes with glucose for uptake and phosphorylation to FDG-6-phosphate by hexokinase. In the myocardium (unlike other organs), FDG-6-phosphate does not undergo further metabolism and remains trapped intracellularly. FDG uptake is increased or preserved in several altered myocardial states that are associated with contractile dysfunction and/or reduced perfusion, thereby indicating the persistence of metabolic activity and hence residual viability with the potential for recovery. Increased or preserved FDG uptake has been observed during ongoing ischemia (*25*), postischemic stunning (*26*), chronic hibernation (*27*) and after heart transplantation (*28*). In patients with coronary artery disease, all these conditions imply jeopardized myocardium requiring therapy, most often by revascularization.

Although the clinical value of FDG uptake by myocardial tissue remains undisputed, there is considerable controversy regarding the value of FDG as a quantitative probe for the measurement of myocardial glucose utilization. One issue is the adequacy of the tracer kinetic model, in particular the stability of the lumped constant that relates uptake and phosphorylation kinetics of FDG and glucose (*29*). For instance, ischemia affects the translocation of glucose transporters, the expression of transporter subtypes and the affinity of hexokinase, all of which may affect the lumped constant (*30*). The use of FDG also requires steady-state metabolic conditions during tracer delivery, not easily achieved in clinical practice. Because the myocardium uses several substrates (*31*), including free fatty acids (FFAs), glucose, lactate, ketone bodies or amino acids, depending on fuel delivery and hormonal status, adequate image quality can only be obtained by increasing glucose availability. Most glucose-loading protocols do not ensure stability of the hormonal and metabolic milieu such that the quantification of glucose metabolism cannot be easily obtained.

GLUCOSE LOADING

One of the major drawbacks to the widespread use of FDG cardiac imaging has been the complexity of the glucose-loading protocol. The long patient preparation time observed with oral glucose loading is due in large part to the occurrence of abnormal glucose tolerance and insulin resistance in a significant proportion of patients with ischemic heart disease (*32,33*). The presence of impaired glucose tolerance and insulin resistance cannot be determined prospectively at the time of the procedure, but patients with a fasting blood glucose of greater than 100 mg/dl have a high likelihood of having diabetes or impaired glucose tolerance (*34*). The need for frequent blood glucose monitoring and supplemental insulin administration, using an oral glucose-loading protocol, results in significant logistical problems.

In nondiabetic patients, a threefold increase in myocardial glucose utilization occurs after a 30-min infusion of a fixed concentration of glucose-insulin-potassium (GIK) solution (*35*). Martin et al. (*36*) performed DISA SPECT imaging on 98 consecutive nondiabetic patients after preparation with a fixed concentration GIK infusion administered at a standardized rate of 3 ml/kg/hr, corresponding to an insulin infusion of 1.78 mU/kg/min and a glucose infusion of 10 mg/kg/min. The GIK solution consisted of 16 U of aqueous regular insulin in 500 ml 20% dextrose plus 10 mEq KCl in a glass bottle. Each patient was primed with an intravenous bolus injection of 5 U regular insulin and 50 ml 20% dextrose immediately before initiation of the GIK infusion. Blood glucose was monitored at 15 and 30

min. If blood glucose rose above 200 mg/dl, additional intravenous bolus injections of regular insulin were administered (5–10 U). During the stress protocol and image acquisition, 20% dextrose without insulin was infused at 2–3 ml/kg/hr, and the patient was fed a snack on completion of the acquisition to avoid delayed insulin-induced hypoglycemia. Using the GIK infusion protocol, the mean preparation time for the average patient was decreased by approximately 1 hr compared to oral glucose loading, and scan quality was consistently good to excellent, with only 1% of images being uninterpretable. This compares favorably to the 2%–33% incidence of uninterpretable images reported in the literature with oral glucose loading. An additional advantage of the GIK protocol compared to oral loading is the ability to continue the infusion when logistical delays occur, without sacrificing good image quality. Standardized infusion of a fixed concentration of GIK before FDG administration and continued during myocardial FDG uptake is an effective yet simple method of obtaining consistently good-to-excellent quality FDG cardiac scans. This method is preferable to conventional oral glucose loading because patient preparation time is decreased and image quality is improved.

Uninterpretable FDG scans have been reported in 10%–28% of diabetic patients (*37,38*). Consequently, diabetic subjects are prepared using a formal or modified euglycemic hyperinsulinemic clamp protocol (*39–42*). Oral glucose loading and the GIK loading protocol are not appropriate for use in diabetic patients. Using a modified euglycemic hyperinsulinemic clamp, several investigators have reported excellent image quality in small populations of diabetic patients (*39–42*). After attaining near-euglycemia by the infusion of intravenous insulin at 4 mU/kg/min, glucose is administered intravenously at a rate of 6 mg/kg/min. Blood glucoses are monitored every 5–10 min, and the glucose infusion rate is altered appropriately to achieve blood glucoses of 80–150 mg/dl. FDG is injected after approximately 20 min of "stable" blood glucose. This technique is adequate for clinical work but remains labor intensive.

NICOTINIC ACID

Knuuti et al. (*43*) have demonstrated that oral administration of a nicotinic acid derivative (acipimox) may be an alternative to either oral glucose loading or euglycemic clamping. Acipimox inhibits peripheral lipolysis, thus reducing plasma FFA levels, and has a mechanism of action which is similar to that postulated for nicotinic acids but is 20 times more potent; it also has a longer duration of action as compared to nicotinic acids (*44*). After oral ingestion, peak plasma levels of the drug are reached within 2 hr (*45*).

Knuuti et al. (*43*) have performed a direct comparison between hyperinsulinemic euglycemic clamping and acipimox in 12 patients with coronary artery disease. The clamping protocol was performed according to well-described standards (*46*). For the acipimox protocol, patients were administered 250 mg acipimox orally 3 hr before FDG injection, followed by a second dose of 250 mg acipimox 1.5 hr before FDG injection. As expected, insulin levels were high during clamping and low after acipimox administration. Plasma levels of FFA were comparably low after acipimox and during clamping. FDG activity in the myocardium and blood was higher after acipimox as compared to the clamping protocol. The myocardium-to-blood ratio (frequently used as a measure of image quality) was comparable after both approaches. No side effects of acipimox (besides flushing) were observed. The myocardial FDG uptake patterns were compared visually and showed no significant differences.

Bax et al. (*47*) recently compared all three approaches (acipimox, clamping and oral loading) in eight nondiabetic patients (seven with coronary artery disease). The oral glucose-loading and clamping protocols were performed according to established criteria (*46,48*). The acipimox protocol was slightly modified from that used by Knuuti et al. (*43*) in that a single dose (250 mg) of acipimox was administered, and patients received a carbohydrate-and-protein-enriched meal to stimulate endogenous insulin release, thereby further promoting myocardial and peripheral FDG uptake. FFA levels were low with acipimox and during clamping but were significantly higher after oral glucose loading. Insulin levels were raised in all three protocols (Table 4). The myocardium-to-blood activity ratios were comparable after acipimox and during clamping but significantly lower after oral glucose loading. The FDG clearance rate from blood was significantly lower after oral loading compared to acipimox and clamping (T $[\frac{1}{2}]$ oral load = 16.2 min, T $[\frac{1}{2}]$ acipimox = 10.7 min and T $[\frac{1}{2}]$ clamp = 8.1 min). Visually, the FDG images were superior after clamping and acipimox compared to oral glucose loading. Although Bax et al. (*47*) included only nondiabetic patients, Knuuti et al. (*43*) included seven patients with diabetes mellitus type II. In these patients, the image quality was also equivalent after acipimox administration compared to clamping.

TABLE 4
Substrate Levels During Clamping, After Acipimox Administration and After Oral Glucose Loading*

	Glucose (mmol/liter)	FFA (mmol/liter)	Insulin (mU/liter)
Clamping	5.1 ± 0.8	0.04 ± 0.01	109.8 ± 34.6
Acipimox	5.1 ± 0.6	0.03 ± 0.01	66.3 ± 24.3†
Oral load	8.0 ± 1.7†	0.16 ± 0.07†	101.3 ± 17.1

*Based on data from reference *47*.
†$p < 0.01$ vs. other protocols; FFA = free fatty acid.

Limited results with cardiac FDG imaging after acipimox administration are encouraging, but larger studies are needed in patients with and without diabetes mellitus. Still, the available evidence, although limited, shows that good image quality can be obtained using acipimox (comparable to clamping and superior to oral glucose loading) and may be sufficient for clinical assessment of viability.

IMAGING PROTOCOLS

Identification of hibernating myocardium with FDG can be performed using either sequential or DISA imaging protocols (*17,19–21*).

Sequential Acquisition

Assessment of hibernating myocardium with PET requires the performance of sequential imaging to detect regions of myocardial perfusion/metabolism mismatch. PET cameras that are not capable of performing simultaneous transmission/emission tomography require a separate transmission scan. The development of coincidence detection with simultaneous attenuation correction, using DHC scintillation cameras, has permitted cardiac viability studies to be obtained using DHC with resolution equivalent to PET. However sequential imaging using perfusion/metabolism mismatch to identify hibernating myocardium is still necessary.

Both Burt et al. (*17*) and Bax et al. (*19*) have demonstrated the ability to identify hibernating myocardium using sequential ^{201}Tl/FDG SPECT imaging. Data generated by Bax et al. using ^{201}Tl/FDG imaging to identify hibernating myocardium have

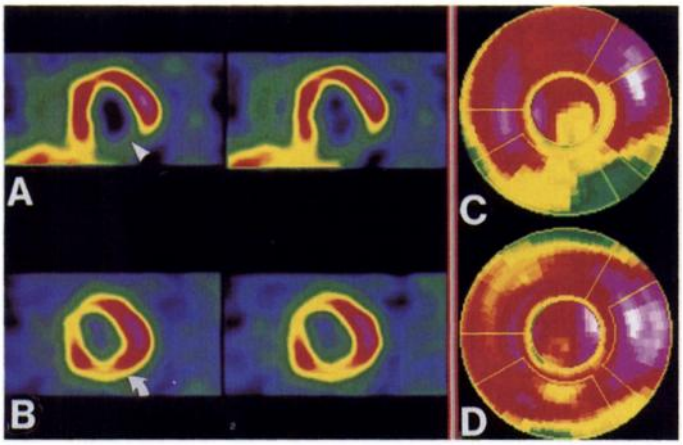

FIGURE 3. A 63-yr-old patient with history of chronic ischemic heart disease (LVEF = 20%) referred for DISA SPECT to ascertain presence of hibernating myocardium. Stress ^{99m}Tc-MIBI (A) and rest FDG short-axis (B) images detect a region of inferolateral mismatch. Perfusion (C) and metabolic bull's eye (D) images detect multiple viable segments in ischemic inferolateral wall. Patient underwent multivessel coronary artery bypass grafting after DISA SPECT. Repeat echocardiogram 3 mo postsurgery revealed normal inferolateral wall motion and LVEF of 40%. Images were obtained with 90° variable-angle camera.

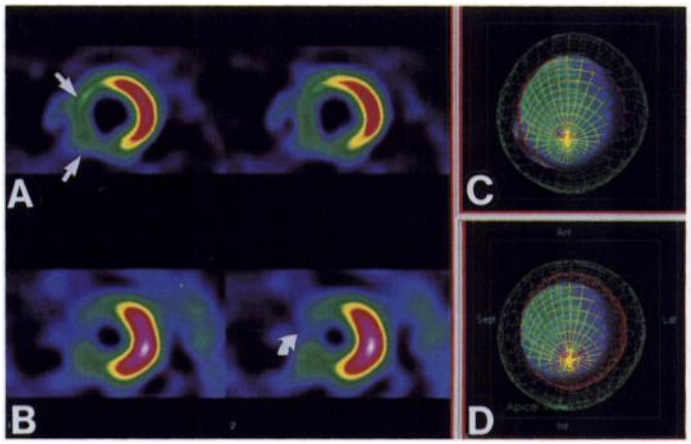

FIGURE 4. A 55-yr-old man with past history of myocardial infarction was referred for DISA SPECT after an episode of atypical chest pain. Stress ^{99m}Tc-MIBI (A) and rest FDG short-axis (B) images detected anteroseptal myocardial scar (arrows). End-diastolic (C) and end-systolic (D) quantitative gated SPECT (LVEF = 27%) acquired during DISA protocol demonstrate normal lateral wall motion with diffuse LV hypokinesis. Images were obtained with 90° variable-angle camera.

been shown to be comparable to results obtained with ^{13}N-labeled ammonia/FDG PET (*49*).

Simultaneous Acquisition

DISA cardiac studies with FDG/^{99m}Tc-MIBI SPECT have been performed to evaluate hibernating myocardium and provide PET-comparable images and results. Delbeke et al. (*21*) reported their experience in a series of patients undergoing DISA SPECT using a rest perfusion–rest metabolism ^{99m}Tc-MIBI/FDG SPECT imaging protocol. With stenosis greater than 70% used as the diagnostic criterion for coronary artery disease, DISA SPECT had a sensitivity of 100% and a positive predictive value of 93%. Sandler et al. (*20*) described the use of DISA SPECT to evaluate myocardial ischemia and viability according to a rest metabolism–stress perfusion protocol using FDG/^{99m}Tc-MIBI (Fig. 3). When stenosis of greater than 70% was used as the diagnostic criterion for coronary artery disease, DISA SPECT had a sensitivity of 100% specificity of 88%, positive predictive value of 93%, negative predictive value of 100% and an accuracy of 96% (*20*). The development of 90° dual-head acquisition using high-resolution ultrahigh-energy collimators with $\frac{5}{8}$ in. thick crystals has permitted cardiac gating with assessment of wall motion and geometric ejection fraction values to be obtained with DISA SPECT (Fig. 4).

DATA ANALYSIS

Several approaches to analyze FDG data have been described, including absolute quantification, semiquantitative analysis and visual analysis.

Absolute Quantification of Myocardial FDG Uptake to Assess Regional Glucose Utilization

This approach requires dynamic PET imaging and is, thus far, not possible with FDG SPECT. Absolute myocardial glucose utilization can be calculated using the Patlak analysis (*50*). This approach requires arterial plasma sampling and was adapted by Ghambir et al. (*51*) using blood-pool and myocardial FDG time-activity curves. Although permitting assessment of absolute myocardial glucose utilization, the approach remains complex and suffers from the restrictions imposed by the use of the lumped constant.

Semiquantitative Analysis Using Static FDG Imaging

Most cardiac FDG studies have used static imaging and some form of semiquantitative analysis. In the initial study by Marshall et al. (*25*), circumferential profiles were compared with reference values obtained in normal individuals. Regions with diminished flow and normal or increased FDG uptake were considered to represent viable myocardium (flow-metabolism mismatch), whereas regions with concordantly reduced flow and FDG uptake (flow-metabolism match) were considered to represent scar tissue. This approach is based on "slice-analysis," whereas more recent reports have used the profiles of all short-axis slices displayed in polar maps (*52*). This approach allows evaluation of the entire LV in a single image. The flow and FDG polar maps can be compared with separate normal databases (*52*), or the regional FDG uptake can be normalized to the region with maximum flow.

Some investigators have used FDG in isolation to identify viable myocardium (*53,54*). These studies have normalized regional FDG uptake to the maximum tracer uptake per slice or in the entire polar map. Viable tissue is considered to be present when the normalized FDG activity exceeds 50%. While combined flow FDG imaging has been shown to predict functional recovery after revascularization (*55*), the use of a 50% cutoff criterion has never been validated against revascularization.

Visual Analysis

Recently, Vom Dahl et al. (*56*) analyzed their FDG and flow data visually and compared the results with functional recovery after revascularization. The authors scored the segments on a 4-point scale, ranging from normal tracer uptake to absent tracer uptake. The segments with a flow-metabolism match did not recover function after revascularization, and the majority of the segments with a flow-metabolism mismatch demonstrated an improvement in function. Notably, the segments with a mild reduction in flow and FDG uptake did not recover function after revascularization. Hence, FDG imaging alone would not have resulted in adequate prediction of functional recovery. In their conclusion, the authors emphasized that visual analysis may be preferred for routine clinical imaging.

CLINICAL VALUE OF FDG SPECT

Assessment of myocardial viability with FDG to identify injured but viable myocardium in patients with severe coronary artery disease and ischemic LV dysfunction, but who are

eligible for coronary revascularization, is an all-important indication for FDG imaging (*57*). It has now become clear that impaired LV function is not necessarily an irreversible process, because recovery of LV function after revascularization has been demonstrated, even in severely dyssynergic myocardial regions (*58*). Hibernation and repetitive stunning have been introduced to explain a situation of reversibly impaired LV function (*27,59*). Hence, in the presence of jeopardized but viable myocardium, improvement of LV function can be expected after revascularization, whereas no improvement will occur when the dysfunction is caused by scar tissue. While patients with a poor LV function are at high risk for perioperative events, any improvement in LV ejection fraction (LVEF) will have a significant impact on their long-term prognosis (*60*). PET using FDG is considered one of the most accurate techniques to identify injured but viable myocardium (*61*) and select the most appropriate form of therapy (medical, revascularization or heart-transplantation) in patients with impaired LV function.

It has also become apparent that the assessment of viable myocardium in these patients provides important prognostic information. Four studies (*62–65*) using FDG PET have recently emphasized this issue. All of these studies were consistent in showing a high cardiac-event rate in patients with ischemic but viable myocardium who did not undergo revascularization. Although FDG PET provides important clinical information in patients with ischemic LV dysfunction, the restricted availability of the technique does not meet the increasing demand (*66*). The FDG SPECT approach, however, does allow widespread FDG imaging for the assessment of hibernating myocardium.

In a recent study, 55 patients with chronic coronary artery disease and LV dysfunction were evaluated with FDG SPECT before revascularization (*49*). Functional follow-up was obtained 3 mo after revascularization. To allow prediction of functional recovery after revascularization on a regional basis, the LV was divided into 13 segments. Resting echocardiography revealed abnormal wall motion before revascularization in 305 segments; 281 of these segments were adequately revascularized. Three months after revascularization, 94 segments showed improved function, with 80 segments classified viable by FDG SPECT. Conversely, 187 segments did not improve in function after the revascularization, with 120 segments classified nonviable by FDG SPECT. The sensitivity and specificity were 85% and 75%, respectively. In a subset of 22 patients with an LVEF $< 30\%$, the sensitivity and specificity to predict improvement of regional function were 89% and 72%, respectively. The results are in line with data obtained from a pooled analysis of 332 patients undergoing FDG PET, yielding a sensitivity of 88% and a specificity of 73% (*55*).

In the study with FDG SPECT, resting LVEF was also determined before and 3 mo after revascularization. A patient was considered a surgical candidate when three or more dysfunctional segments were classified viable on FDG SPECT. In the patients ($n = 14$) with three or more viable segments, the LVEF improved significantly from 25% ± 6% to 32% ± 6% ($p < 0.01$). Alternatively, in the patients ($n = 8$) with no more than two viable segments, the LVEF remained unchanged (24% ± 6% versus 25% ± 6%) (NS). Although the available data were obtained in a small number of patients, FDG SPECT accurately predicts functional recovery after revascularization.

The most frequently used techniques to assess hibernating myocardium, besides FDG imaging, are ^{201}Tl scintigraphy and low-dose dobutamine echocardiography.

The ^{201}Tl protocols used most frequently include stress-redistribution-reinjection imaging (*67*) and rest-redistribution imaging (*68*). While the reinjection protocol allows detection of both viability and ischemia, rest-redistribution only permits viability assessment. One study compared FDG SPECT with ^{201}Tl reinjection imaging (*69*). Seventeen patients were studied with both techniques before revascularization. Regional wall motion was assessed by echocardiography before and 3 mo after revascularization. The agreement for the detection of viable and nonviable segments between the techniques was 70%. Both approaches had a high sensitivity in predicting improvement of function (93% for ^{201}Tl and 89% for FDG) (Fig. 5). The specificity of FDG SPECT, however, was significantly higher than for ^{201}Tl reinjection (77% versus 43%, $p < 0.05$).

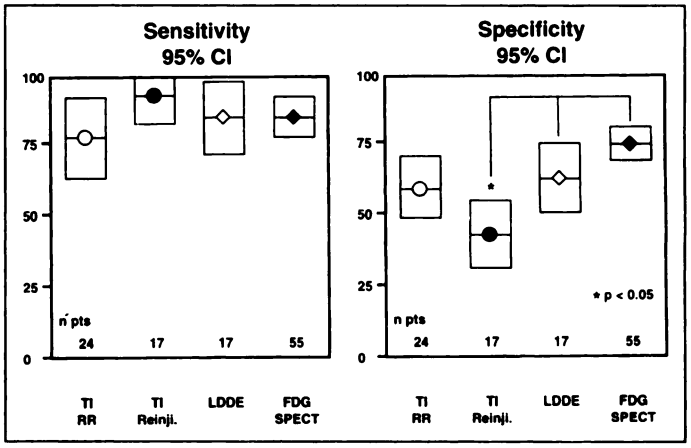

FIGURE 5. Receiver operating characteristic display, indicating sensitivities (left) and specificities (right) with their 95% confidence intervals (squares/rectangles) for various techniques. Data are based on studies that evaluated FDG SPECT versus other techniques, using improvement of function after revascularization as the gold standard for viability (data derived from references *53,75,76*). Sensitivities of different techniques are identical. In these studies, FDG SPECT had the highest specificity. (Tl RR = ^{201}thallium rest-redistribution; Tl Reinj = ^{201}thallium reinjection; LDDE = low-dose dobutamine echocardiography).

Thus far, only preliminary data are available on the comparison between ^{201}Tl rest-redistribution and FDG SPECT (*70*). In 24 patients, both techniques were tested against revascularization. Resting echocardiography was used to evaluate regional contractile function before and after revascularization. A total of 106 dysfunctional segments were revascularized adequately. The sensitivity of FDG SPECT and ^{201}Tl rest-redistribution were comparable: 89% versus 78%. The specificity of FDG SPECT was higher: 81% versus 59% (Fig. 5). Hence, these comparative studies show that FDG SPECT and ^{201}Tl imaging are equally sensitive in predicting functional recovery after revascularization, but the ^{201}Tl protocols tend to overestimate functional recovery (i.e., lower specificity). Pooled analysis of the available ^{201}Tl studies in patients undergoing revascularization has detected the same trend (*55*).

Echocardiography during the infusion of low-dose dobutamine is frequently used to identify injured but viable myocardium. The viable myocardium is characterized by the presence of a contractile reserve, i.e., improvement of wall motion in a segment with resting dysfunction (*71*). Various studies have demonstrated the use of this technique to predict functional recovery after revascularization (*55*). In 17 patients with chronic coronary artery disease and LV dysfunction, both techniques were compared. The agreement for the identification of viable and nonviable segments between the techniques was 80%. The sensitivity and specificity of dobutamine echocardi-

ography were 85% and 63%, respectively, whereas these values were 89% and 77% for FDG SPECT.

CONCLUSION

The introduction of a dual-head variable-angle-geometry scintillation camera equipped with thicker crystals ($\frac{5}{8}$ in.) and high resolution, ultrahigh-energy collimators capable of 511 keV imaging has permitted FDG SPECT to provide information equivalent to PET for the identification of injured but viable myocardium in patients with chronic ischemic heart disease. Accuracy in predicting functional recovery after revascularization with FDG SPECT is comparable to the accuracy of FDG PET. The development of standardized glucose-loading protocols, including GIK infusion, and the potential use of nicotinic acid derivatives have simplified the method of obtaining consistently good-to-excellent quality FDG SPECT cardiac studies. FDG SPECT may become the modality of choice for evaluating injured but viable myocardium because of the enhanced availability of FDG, logistics, patient convenience, accuracy and cost-effectiveness compared to PET.

ACKNOWLEDGMENTS

The authors would like to thank Donna Wagner for preparing the manuscript and Tom Ebers for editing it. We are also grateful to Mary Stoner from Elscint, Inc. for providing the illustrations and John Bobbitt for producing the photographs. This manuscript has been supported by a grant from Elscint Ltd., Haifa, Israel.

REFERENCES

1. Tillisch J, Brunken R, Marshall R, et al. Reversibility of cardiac wall motion abnormalities predicted by positron tomography. *N Engl J Med* 1986;314:884–888.
2. Tamaki N, Yonekura Y, Yamashita K, et al. Positron emission tomography using fluoro-18 deoxyglucose in evaluation of coronary artery bypass grafting. *Am J Cardiol* 1989;64:860–865.
3. Nienaber CA, Brunken RC, Sherman CT, et al. Metabolic and functional recovery of ischemic human myocardium after coronary angioplasty. *J Am Coll Cardiol* 1991;18: 966–978.
4. Marwick TH, Nemec JJ, Lafont A, Salcedo EE, MacIntyre WJ. Prediction by postexercise fluoro-18-deoxyglucose positron emission tomography of improvement in exercise capacity after revascularization. *Am J Cardiol* 1992;69:854–859.
5. Lucignani G, Paolini G, Landoni C, et al. Presurgical identification of hibernating myocardium by combined use of technetium-99m hexakis 2-methoxyisobutylisonitrile single photon emission tomography and fluorine-18 fluoro-2-deoxy-D-glucose positron emission tomography in patients with coronary artery disease. *Eur J Nucl Med* 1992;19:874–881.
6. Carrel Y, Jenni R, Haubold-Reuter S, Schulthess G, Pasic M, Turina M. Improvement of severely reduced left ventricular function after surgical vascularization in patients with preoperative myocardial infarction. *Eur J Cardiothorac Surg* 1992;6:479–484.
7. Eitzman D, Al-Aouar Z, Kanter HL, et al. Clinical outcome of patients with advanced coronary artery disease after viability studies with positron emission tomography. *J Am Coll Cardiol* 1992;20:559–565.
8. Sandler MP, Patton JA. Fluorine 18-labeled fluorodeoxyglucose myocardial single-photon emission computed tomography: an alternative for determining myocardial viability. *J Nucl Cardiol* 1996;3:342–349.
9. Dilsizian V, Bonow RO. Current diagnostic techniques of assessing myocardial viability in patients with hibernating and stunned myocardium. *Circulation* 1993;87: 1–20.
10. Hoflin Ledermann H, Noelpp U, Weinreich R, Rosler H. Routine F-18-2-deoxy-2-fluoro-D-glucose (F-18-FDG) myocardial tomography using a normal large field of view gamma camera. *Angiology* 1989;40:1058–1064.
11. Williams KA, Taillon LA, Start VJ. Quantitative planar imaging of glucose metabolic activity in myocardial segments with exercise thallium-201 perfusion defects in patients with myocardial infarction: comparison with late (24-hour) redistribution thallium imaging for detection of reversible ischemia. *Am Heart J* 1992;124:294–304.
12. Lingen AV, Huijgens PC, Visser FC, et al. Performance characteristics of a 511-keV collimator for imaging positron emitters with a standard gamma-camera. *Eur J Nucl Med* 1992;19:315–321.
13. Bax JJ, Visser FC, Blanksma PK, et al. Comparison of myocardial uptake of F18-fluorodeoxyglucose imaged with positron emission tomography and single photon emission computed tomography. *J Nucl Med* 1996;37:1631–1636.
14. Stoll HP, Hellwin N, Alexander C, Ozbek C, Schieffer H, Oberhausen E. Myocardial metabolic imaging by means of fluorine-18 deoxyglucose/technetium-99m sestamibi dual-isotope single photon emission tomography. *Eur J Nucl Med* 1994;21:1085–1093.
15. Kalff V, Berlangieri SU, van Every B, et al. Is planar thallium 201/F-18 fluorodeoxyglucose imaging a reasonable clinical alternative to PET myocardial viability scanning? *Eur J Nucl Med* 1995;22:625–632.
16. Martin WH, Delbeke D, Patton JA, et al. FDG SPECT: correlation with FDG-PET. *J Nucl Med* 1995;36:988–995.
17. Burt RW, Perkins OW, Oppenheim BE, et al. Direct comparison of fluorine-18-FDG SPECT, fluorine-18-FDG PET and rest thallium-201 SPECT for detection of myocardial viability. *J Nucl Med* 1995;36:176–179.
18. Huitink JM, Visser FC, van Lingen A, et al. Feasibility of planar fluorine-18-FDG imaging after recent myocardial infarction to assess myocardial viability. *J Nucl Med* 1995;36:975–981.
19. Bax JJ, Cornel JH, Visser FC, et al. Reversibility of wall motion abnormalities predicted by SPECT with F18-fluorodeoxyglucose. *J Nucl Med* 1994;35(suppl):136P.
20. Sandler MP, Videlefsky S, Delbeke D, et al. Evaluation of myocardial ischemia using a rest metabolism/stress perfusion protocol with fluorine-18 deoxyglucose/technetium-99m MIBI and dual-isotope simultaneous-acquisition single-photon emission computed tomography. *J Am Coll Cardiol* 1995;26:870–878.
21. Delbeke D, Videlefsky S, Patton JA, et al. Rest myocardial perfusion/metabolism imaging using simultaneous dual-isotope acquisition SPECT with technetium-99m-MIBI/fluorine-18-FDG. *J Nucl Med* 1995;36:2110–2119.
22. Patton JA, Sandler MP, Ohana I, Weinfeld Z. High-energy (511 keV) imaging with the scintillation camera. *RadioGraphics* 1996;16:1183–1194.
23. Yang DC, Ragasa E, Gould L, et al. Radionuclide simultaneous dual-isotope stress myocardial perfusion study using the "three window technique." *Clin Nucl Med* 1993;18:852–857.
24. Siegel S, Dahlbom M. Implementation and validation of a calculated attenuation correction for PET. *IEEE Trans Nucl Sci* 1992;39:1117–1121.
25. Marshall RC, Tillisch JH, Phelps ME, et al. Identification and differentiation of resting myocardial ischemia and infarction in man with positron computed tomography, ^{18}F-labeled fluorodeoxyglucose and N-13 ammonia. *Circulation* 1983;67:766–778.
26. Heyndrickx GR, Wijns W, Degrieck Y, Vandeplassche L, Melin JA. Recovery of regional contractile function and oxidative metabolism in stunned myocardium induced by 1-hour circumflex coronary artery occlusion in chronically instrumented dogs. *Circ Res* 1993;72:901–913.
27. Vanoverschelde JLJ, Wijns W, Depre C, et al. Mechanisms of chronic regional postischemic dysfunction in humans. New insights from the study of noninfarcted collateral-dependent myocardium. *Circulation* 1993;87:1513–1523.
28. Rechavia E, de Silva R, Kushwaha SS, et al. Enhanced myocardial F18-fluoro-2-deoxyglucose uptake after orthotopic heart transplantation assessed by positron emission tomography. *J Am Coll Cardiol* 1997;30:533–538.
29. Harihan R, Bray M, Ganim R, Doenst T, Goodwin GW, Taegtmeyer H. Fundamental limitations of [^{18}F]2-deoxy-2-fluoro-D-glucose for assessing myocardial glucose uptake. *Circulation* 1995;91:2435–2444.
30. Sun D, Nguyen N, DeGrado TR, Schwaiger M, Brosius III FC. Ischemia induces translocation of the insulin-responsive glucose transporter GLUT4 to the plasma membrane of cardiac myocytes. *Circulation* 1994;89:793–798.
31. Camici RG, Ferrannini E, Opie LH. Myocardial metabolism in ischemic heart disease: basic principles and application to imaging by positron emission tomography. *Prog Cardiovasc Dis* 1989;32:217–238.
32. Nuutila P, Koivisto VA, Knuuti J, et al. Glucose-free fatty acid cycle operates in human heart and skeletal muscle in vivo. *J Clin Invest* 1992;89:1767–1774.
33. Black HR. The coronary artery disease paradox: the role of hyperinsulinemia and insulin resistance and implications for therapy. *J Cardiovasc Pharmacol* 1990; 15(suppl):S26–S38.
34. Bennett PH. Definition, diagnosis, and classification of diabetes mellitus and impaired glucose tolerance. In: Kahn CR, Weir GC, eds. *Joslin's diabetes mellitus*, 13th ed. Malvern, PA: Lea & Febiger; 1994:193–200.
35. Rogers WJ, Russell RO, McDaniel HG, Rackley CE. Acute effects of glucose-insulin-potassium infusion on myocardial substrates, coronary blood flow and oxygen consumption in man. *Am J Cardiol* 1977;40:421–428.
36. Martin WH, Jones RC, Delbeke D, Sandler MP. A simplified intravenous glucose loading protocol for fluorine-18-fluorodeoxyglucose cardiac single-photon emission tomography. *Eur J Nucl Med* 1997;24:1291–1297.
37. Vom Dahl J, Hicks R, Lee K, Eitzman D, Alaouar Z, Schwaiger M. Positron emission tomography myocardial viability studies in patients with diabetes mellitus. *J Am Coll Cardiol* 1991;17:121A.
38. Prellwitz J, Vasta M, Sunderland J, Shiue C-Y, Gupta N, Frick M. Investigation of factors influencing FDG myocardial image quality [Abstract]. *J Nucl Med* 1991;32: 1039.
39. Knuuti MJ, Nuutila P, Ruotsalainen U, et al. Euglycemic hyperinsulinemic clamp and oral glucose load in stimulating myocardial glucose utilization during positron emission tomography. *J Nucl Med* 1992;33:1255–1262.
40. Bax JJ, Visser FC, van Lingen A, et al. Feasibility of myocardial F18-fluorodeoxyglucose single photon emission computed tomography in patients with noninsulin-dependent diabetes mellitus. *Nucl Med Commun* 1997;18:200–206.
41. Ohtake T, Yokoyama I, Watanabe T, et al. Myocardial glucose metabolism in noninsulin-dependent diabetes mellitus patients evaluated by FDG-PET. *J Nucl Med* 1995;36:456–463.
42. Schelbert HR. Euglycemic hyperinsulinemic clamp and oral glucose load in stimulating myocardial glucose utilization during positron emission tomography. *J Nucl Med* 1992;33:1263–1266.
43. Knuuti MJ, Yki-Järvinen H, Voipio-Pulkki LM, et al. Enhancement of myocardial [fluorine-18] fluorodeoxyglucose uptake by a nicotinic acid derivative. *J Nucl Med* 1994;35:989–998.
44. Fuccella LM, Goldaniga GC, Lovisolo PP. Inhibition of lipolysis by nicotinic acid and by acipimox. *Clin Pharmacol Ther* 1980;28:790.
45. Musatti L, Maggi E, Moro E, Valzelli G, Tamassia V. Bioavailability and pharmacokinetics in man of acipimox, a new antilipolytic and hypolipemic agent. *J Int Med Res* 1981;9:381–386.
46. Knuuti H, Nuutila P, Ruotsalainen U, et al. Euglycemic hyperinsulinemic clamp and oral glucose load in stimulating myocardial glucose utilization during positron emission tomography. *J Nucl Med* 1992;33:1255–1262.
47. Bax JJ, Veening MA, Visser FC, et al. Optimal metabolic conditions during FDG

imaging: a comparative study using different protocols. *Eur J Nucl Med* 1997;24:35–41.
48. Gropler RJ. Methodology governing the assessment of myocardial glucose metabolism by PET and fluorine 18-labeled FDG. *J Nucl Cardiol* 1994;1:S4–S14.
49. Bax JJ, Cornel JH, Visser FC, et al. Prediction of improvement of contractile function in patients with ischemic ventricular dysfunction after revascularization by F18-fluorodeoxyglucose SPECT. *J Am Coll Cardiol* 1997;39:377–384.
50. Patlak CS, Blasbeg RG. Graphical evaluation of blood-to-brain transfer constants from multiple-time uptake data: generalizations. *J Cereb Blood Flow Metab* 1985;5:584–590.
51. Gambhir SS, Schwaiger M, Huang SC, et al. Simple noninvasive quantification method for measuring myocardial glucose utilization in humans employing positron emission tomography and fluorine-18 deoxyglucose. *J Nucl Med* 1989;30:359–366.
52. Porenta G, Kuhle W, Czernin J, et al. Semiquantitative assessment of myocardial blood flow and viability using polar map displays of cardiac PET images. *J Nucl Med* 1992;33:1623–1631.
53. Baer FM, Voth E, Schneider CA, Theissen P, Schicha H, Sechtem U. Comparison of low-dose dobutamine-gradient-echo magnetic resonance imaging and positron emission tomography with [^{18}F]fluorodeoxyglucose in patients with chronic coronary artery disease. A functional and morphological approach to the detection of residual myocardial viability. *Circulation* 1995;91:1006–1015.
54. Chan RKM, Lee KJ, Calafiore P, Berlangieri SU, McKay WJ, Tonkin AM. Comparison of dobutamine echocardiography and positron emission tomography in patients with chronic ischemic left ventricular dysfunction. *J Am Coll Cardiol* 1996;27:1601–1607.
55. Bax JJ, Wijns W, Cornel JH, Visser FC, Boersma E, Fioretti PM. Accuracy of currently available techniques for prediction of functional recovery after revascularization in patients with left ventricular dysfunction due to chronic coronary artery disease: comparison of pooled data. *J Am Coll Cardiol* 1997;30:1451–1460.
56. Vom Dahl J, Eitzman DT, Al-Aouar ZR, et al. Relation of regional function, perfusion and metabolism in patients with advanced coronary disease undergoing surgical revascularization. *Circulation* 1994;90:2356–2366.
57. Ritchie JL, Bateman TM, Bonow RO, et al. Guidelines for clinical use of cardiac radionuclide imaging. *Circulation* 1995;91:1278–1303.
58. Elefteriades JA, Tolis G, Levi E, Mills LK, Zaret BL. Coronary artery bypass grafting in severe left ventricular dysfunction: excellent survival with improved ejection fraction and functional state. *J Am Coll Cardiol* 1993;22:1411–1417.
59. Ross JR Jr. Myocardial perfusion-contraction matching: implications for coronary heart disease and hibernation. *Circulation* 1991;83:1076–1083.
60. Mock M, Ringqvist I, Fisher LD, et al. Survival of medically treated patients in the coronary artery surgery study (CASS) registry. *Circulation* 1982;66:562–568.
61. Maddahi J, Schelbert H, Brunken R, Di Carli M. Role of Tl-201 and PET imaging in evaluation of myocardial viability and management of patients with coronary artery disease and left ventricular dysfunction. *J Nucl Med* 1994;35:707–715.
62. Di Carli M, Davidson M, Little R, et al. Value of metabolic imaging with positron emission tomography for evaluating prognosis in patients with coronary artery disease and left ventricular dysfunction. *Am J Cardiol* 1994;73:527–533.
63. Eitzman D, Al-Aouar ZR, Kanter HL, et al. Clinical outcome of patients with advanced coronary artery disease after viability studies with positron emission tomography. *J Am Coll Cardiol* 1992;20:559–565.
64. Vom Dahl J, Altehoefer C, Sheehan FH, et al. Effect of myocardial viability assessed by technetium-99m-sestamibi SPECT and fluorine-18-FDG PET on clinical outcome in coronary artery disease. *J Nucl Med* 1997;38:742–748.
65. Marwick TH, MacIntyre WJ, Lafont A, Nemec JJ, Salcedo EE. Metabolic responses of hibernating and infarcted myocardium to revascularization. *Circulation* 1992;85:1347–1353.
66. Camici PG, Wijns W, Borgers M, et al. Pathophysiological mechanisms of chronic reversible left ventricle dysfunction due to coronary artery disease (hibernating myocardium). *Circulation* 1997;96:3205–3214.
67. Dilsizian V, Rocco TP, Freedman NMT, Leon MB, Bonow RO. Enhanced detection of ischemic but viable myocardium by the reinjection of thallium after stress-redistribution imaging. *N Engl J Med* 1990;323:141–146.
68. Ragosta M, Beller GA, Watson DD, Kaul S, Gimple LW. Quantitative planar rest-redistribution ^{201}Tl imaging in detection of myocardial viability and prediction of improvement in left ventricular function after coronary bypass surgery in patients with severely depressed left ventricular function. *Circulation* 1993;87:1630–1641.
69. Bax JJ, Cornel JH, Visser FC, et al. Prediction of recovery of myocardial dysfunction after revascularization: comparison of fluorine-18 fluorodeoxyglucose/thallium-201 SPECT, thallium-201 stress-reinjection SPECT and dobutamine echocardiography. *J Am Coll Cardiol* 1996;28:558–565.
70. Bax JJ, Cornel JH, Visser FC, Fioretti PM, van Lingen A, Visser CA. Comparison of thallium-201 rest-redistribution SPECT and FDG SPECT in predicting functional recovery after revascularization. *J Am Coll Cardiol* 1996;27(suppl A):300A.
71. Cornel JH, Bax JJ, Fioretti PM. Assessment of myocardial viability by dobutamine stress echocardiography. *Curr Opin Cardiol* 1996;11:621–626.